High performance transparent silver grid electrodes for organic photovoltaics fabricated by selective metal condensation

Philip Bellchambers[a1], Charlie Henderson[aγ1], Szymon Abrahamczyk[b], Seungsoo Choi[c], Jin-Kyun Lee[c,d] and Ross A. Hatton[a*]

[a]Department of Chemistry, University of Warwick, Coventry, CV4 7AL, UK.

[b]AS CDT, University of Warwick, Coventry, CV4 7AL, UK.

[c]Program in Environment and Polymer Engineering, Inha University, Incheon 22212, South Korea.

[d]Department of Polymer Science and Engineering, Inha University, Incheon 22212, South Korea.

[γ]Current address: Department of Physics, Imperial College London, London, SW7 2AZ, UK.

1. These authors contributed equally to the work.

*Corresponding author: ross.hatton@warwick.ac.uk

Abstract

We report silver grid electrodes on glass and flexible plastic substrates with performance that exceeds that of commercial indium-tin oxide (ITO) coated glass and show their suitability as a drop-in replacement for ITO glass in solution processed organic photovoltaics (OPVs). When supported on flexible plastic substrates these electrodes are stable towards repeated bending through a small radius of curvature over tens of thousands of cycles. The grid electrodes are fabricated by the unconventional approach of condensation coefficient modulation using a perfluorinated polymer shown to be far superior to the other compounds used for this purpose to date. The very narrow line-width and small grid pitch that can be achieved also opens the door to the possibility of using grid electrodes in OPVs without a conducting PEDOT:PSS layer to span the gaps between grid-lines.

Introduction

Photovoltaics (PVs) based on silicon and cadmium telluride are set to be the dominant PV technologies for large-scale electricity generation this century.[1] There are however important applications in buildings and transportation for which they are unsuitable as a result of the inherent brittleness of these inorganic semiconductors at the thickness needed to achieve optimal device efficiency, which makes them poorly compatible with flexible substrates. These classes of PV are also

This article has been accepted for publication and undergone full peer review but has not been through the copyediting, typesetting, pagination and proofreading process, which may lead to differences between this version and the Version of Record. Please cite this article as doi: 10.1002/adma.202300166.

limited in the extent to which their colour and transparency can be engineered and they do not harvest indoor light efficiently.[2–4] The need for efficient indoor PVs is primarily motivated by the emergence of the internet of things, which will require power sources for indoor wireless sensor networks.[5] In contrast, PVs devices based on organic semiconductors can be processed at low temperature (< 150˚C) onto flexible plastic substrates, offer the possibility of colour tuneablilty, transparency across the visible spectrum and high power conversion efficiency under indoor lighting conditions.[4,6,7] In addition, OPVs are expected to have the lowest energy payback time of all PV technologies which, combined with the absence of toxic elements, means that they are likely to be the most sustainable PV technology.[8] The Achilles heel of OPVs for practical applications is the relatively poor long term stability, although recently extrapolated intrinsic lifetimes equivalent to 30 years outdoor exposure have been reported for solution processed OPVs and so it seems likely that sufficient stability for applications with a lifetime of ≥ 10 years is within reach. [9]

A key bottleneck to OPVs achieving their full potential, both in terms of the range of potential applications and the cost advantage over PV technologies, is the absence of a high-performance transparent electrode compatible with flexible plastic substrates which can be fabricated in a way that is practical at large area.[10] With the dramatic progress in power conversion efficiency and stability of OPVs made in the past decade, the need for a suitable transparent electrode is increasingly apparent.[11] Materials that offer high (> 85%) transparency across that part of the spectrum of most relevance to PVs (i.e. wavelengths 400 - 1000 nm) that are also sufficiently conductive for large area applications are rare because the free electrons that give rise to high electrical conductivity in most conductors also couple strongly with the oscillating electric component of visible light.[12] To date the vast majority of published reports pertaining to OPVs relate to device architectures in which light enters the device through an indium-tin oxide (ITO) coated glass substrate fabricated by sputter deposition of ITO onto glass followed by annealing at > 300°C to achieve a transparency (~ 90%) and sheet resistance of 15 Ω sq^{-1}.[13,14] Due to its dominance as the transparent electrode used in OPV research, the performance of ITO glass is effectively the gold standard for transparent electrodes used in small area (< 1 cm^2) OPVs. The performance of transparent electrodes is typically quantified in terms of a figure-of-merit (FoM) defined as the ratio of the direct current conductivity (σ_{dc}) to the optical conductivity at a given wavelength ((λ)): Supporting Information, Equation S1.[15] For ITO glass the FoM is ~400. However, this excellent performance is only achieved if the ITO film is thermally annealed at > 300°C which makes it poorly compatible with low cost, flexible transparent plastic substrates such as polyethylene terephthalate (PET). Whilst ITO films on plastic are commercially available, they are extremely fragile due to the brittle ceramic nature of ITO and have performance substantially below that achieved on glass as a result of the restriction on the annealing temperature imposed by the use of a plastic substrate. Furthermore, for OPV devices with an area of ≥ 1 cm^2 the sheet resistance of the transparent electrode needs to be well below 10 Ω sq^{-1} to avoid unacceptable parasitic resistive loses,[16,17] and so the absence of a viable alternative to ITO is a serious limitation to the commercialization of OPVs.[10]

Whilst many alternatives to ITO glass have been proposed that are compatible with flexible substrates, including conducting polymers,[18,19] ultra-thin metal films,[20–23] metal nanowires,[24–26] and metal grids,[16,27,28] very few achieve performance comparable to ITO glass.[12,29] To date transparent electrodes based on solution processed silver (Ag) nanowires, or Ag grids offer the

closest performance to ITO glass.[12,29,30] Ag nanowires are relatively costly to synthesize and films of Ag nanowires can suffer from poor contact stability at the junction between nanowires.[12,29,31,32] However, in recent years substantive improvements in the contact stability between spin cast Ag nanowires have been reported[30,33], enabling the fabrication of robust Ag nanowire electrodes on plastic with a sheet resistance of ~10 Ω sq^{-1} and transparency of ~92 - which corresponds to a FoM of 416.[30] Metal grid electrodes have the advantage of zero contact resistance between metal lines and can be fabricated by depositing colloidal Ag into the pre-etched grooves in the plastic substrate followed by removal of excess Ag nanoparticles.[34,35] Unfortunately using this process the utilization of Ag is quite low and the Ag nanoparticles cannot be compactly filled into the grooves.[34,35] Ag grid fabrication is possible by direct printing from colloidal Ag solutions followed by sintering to fuse the nanoparticles together[36], or by selective removal of Ag from a Ag film by etching[37], or by electrochemical deposition[38,39]. The latter has the advantage that it enables deposition of Ag only where it is needed, but is an inherently chemical intensive and slow batch process. Similarly, etching Ag films to make grids is a slow batch process and uses harmful chemical etchants.[37] Using the conventional printing techniques of screen, inkjet and flexographic printing to fabricate Ag grids from colloidal Ag inks the minimum line-width achievable is > 10 μm and so high transparency can only be achieved with large spacing between grid lines (i.e. grid pitch).[40] One innovative fabrication process that has been developed to address these limitations is bubble-assisted electrode assembly, where capillary forces are harnessed to fabricate compact Ag grids with almost 100% utilization of metallic inks.[41] Using that approach flexible electrodes with a sheet resistance of 7.9 Ω sq^{-1} with 85% transparency have been reported, although the process of electrode fabrication is relatively complex and the scalability is yet to be proven.[41]

In 2019 we reported an entirely different approach to fabricating patterned Ag films, based on the discovery that an extremely thin (≥ 10 nm) printed layer of perfluorinated silane can prevent condensation of Ag vapor deposited under vacuum, such that Ag is selectively deposited only where the perfluorinated silane layer is not.[42] The beauty of this approach is that vacuum evaporation of metals to form thin films is proven as a low cost metal deposition method by the packaging industry, and the shape and dimensions of the features deposited is limited only by the printing method used to deposit the patterned perfluorinated silane layer. This approach also avoids metal waste and the use of harmful chemical etchants and solvents needed for conventional lithographic processes. In 2020 we used this approach to fabricate embedded Ag grid electrodes on flexible plastic substrate with an average far-field transparency of 77% over the wavelength range 400 - 1100 nm and a sheet resistance of 20 Ω sq^{-1} on flexible PET substrates.[43] The innovation in that work was the use a microcontact printed perfluorinated polymethacrylate (poly(1H,1H,2H,2H-perfluorodecyl methacrylate) [PFDMA]) in place of the perfluorinated silane, which enabled a higher degree of control over thin film deposition. Microcontact printing has the advantage that it enables micron-sized grid linewidths which are >10 times narrower than can be achieved using the conventional printing techniques of screen, inkjet and flexographic printing. It is also compatible with roll-to-roll processing and can be scaled to large area at low cost.[44,45] Unfortunately, the time taken to deposit the patterned PFDMA layer by microcontact printing was ~ 10 seconds, which is not compatible with continuous roll-to-roll processing, and the electrode FoM was not competitive with ITO glass; 68 *vs* ~400.

Here we report the development of a new perfluorinated polymer for this application that differs from PFDMA by only two -CF_2- units (Supporting Information, Table S1) but imparts a dramatically improved performance, enabling the fabrication of Ag grid electrodes on plastic and glass substrates with a FoM that exceeds that of ITO glass. Unlike its forerunner, PFOMA transfers instantly from the PDMS stamp to the receiving substrate, which means that it can be used as part of a continuous roll-to-roll fabrication process. We show that the performance of these electrodes as the transparent electrode in solution processed OPVs is comparable to that of devices fabricated on ITO glass electrode, proving its viability as a competitive alternative.

Results and Discussion

Figure 1 shows a schematic of the electrode fabrication process together with the structure of the perfluorinated polymer used to achieve selective Ag deposition in this work; poly(3,3,4,4,5,5,6,6,7,7,8,8,8-tridecafluorooctylmethacrylate (PFOMA). PFOMA was synthesized using a one-step uncontrolled radical polymerization from 1*H*,1*H*,2*H*,2*H*-perfluorooctyl methacrylate (FOMA) in the solvent benzotrifluoride (Supporting Information Figure S1). Microcontact printing is the method of choice for printing patterned films of PFOMA due to the very small feature size that can be achieved using this printing method.[46,47] Microcontact printing uses a polydimethylsiloxane (PDMS) stamp loaded with a thin film of the material to be printed. Due to the unique viscoelastic properties of PDMS the stamp is capable of forming an intimate conformal contact with the receiving substrate in a fraction of a second.[48] When the PDMS stamp is dosed with a thin layer of polymer transfer of the polymer layer from the stamp to the receiving substrate occurs provided the cohesion energy density between the receiving substrate and the polymer exceeds that between the polymer and PDMS stamp.[49] When the surface energy of two materials is known the cohesion energy density between them can be estimated using Equation S2 (Supporting Information).[49] The surface energy of PFOMA and its forerunner PFDMA were determined using the static contact angles for water and *n*-hexadecane and the Owens–Wendt–Rabel–Kaelble equation, to be 10.1 ± 0.3 and 11.1 ± 0.2 mN m^{-1} respectively. The surface energies of PDMS, silicon and glass have been reported elsewhere: Supporting Information, Table S3.[50–52] It is evident from the cohesion energy densities in Table S2 (Supporting Information) that transfer of both PFOMA and PFDMA from the PDMS stamp to glass, PET and a silicon wafer should occur. In practice, PFOMA is transferred immediately on contact with all three of these substrate types and so the printing process is compatible with roll-to-roll processing. Conversely, PFDMA takes ~10 seconds to achieve reproducible transfer to the same substrates, making it unsuitable for roll-to-roll processing.[43] Since both PFOMA and PFDMA do not form chemical bonds with glass, silicon wafer or PET, and there is no significant difference in cohesion energies between them and any of the aforementioned substrates (Supporting Information, Table S2), the stark difference in ease with which they are transferred must relate to another parameter. The AFM force spectroscopy measurements shown in Figure S2 (Supporting Information) show that the surface of the PFOMA film is substantially softer than PFDMA, since the force needed to achieve the same cantilever deflection is lower, consistent with the lower melting point of the former; 65-83°C *vs.* 90-98°C measured using the capillary method (Supporting Information S3 and reference 36). These conclusions are corroborated by the results of differential scanning calorimetry measurements; Supporting Information Figure S4, which show that PFDMA is semi-crystalline, exhibiting both a glass transition temperature (~39°C) and well-defined melting

point peak. Conversely, for PFOMA there is no evidence of a crystalline phase and the glass transition temperature is > 10°C lower than that of PFDMA: < 27°C *vs* ~39°C. It is therefore concluded that the PFOMA film supported on PDMS stamp forms a conformal contact with the receiving substrate more quickly than PFDMA, enabling more rapid transfer.

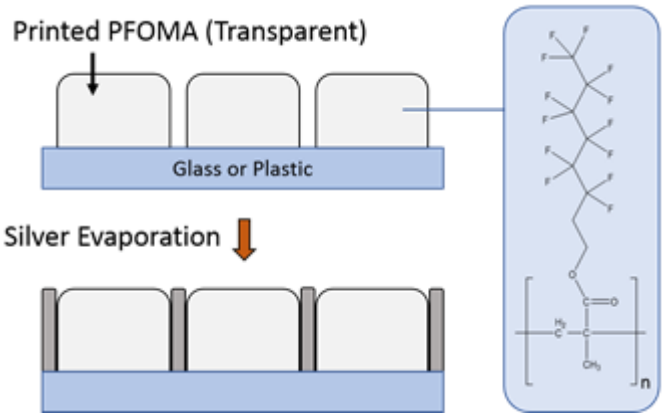

Figure 1: Schematic depiction of the selective metal deposition process to produce an embedded grid electrode.

The ability of micro-contact printed films of PFOMA (e.g. as shown in Supporting Information Figure S5) to resist Ag condensation is quantified in terms of the condensation coefficient *C*. To determine *C* a grid of PFOMA was microcontact printed onto a silicon wafer so that there are regions of PFOMA (i.e. the grid lines) and PFOMA-free regions (i.e. grid apertures) in close proximity. These different regions were then probed using spatially resolved energy dispersive X-ray spectroscopy (EDXS). Using the most intense peak in the Ag EDXS spectrum *C* is defined as the ratio of the Ag peak intensity acquired from a region coated with PFOMA to that acquired from an adjacent PFOMA free area. In the first instance, to enable direct comparison with the efficacy of PFDMA reported previously,[43] 50 nm of Ag was thermally evaporated. It is evident from Figure 2 that for substrate temperatures of greater than ~ 90°C the amount of Ag condensed on the PFOMA is below the detectable limit, which is not achieved using PFDMA even for much higher substrate temperatures. There is also no significant difference in *C* when the PFOMA thickness is increased from 40 nm to 80 nm (Supporting Information, Figure S6), which shows that 40 nm is above the critical thickness of PFOMA needed to resist Ag vapor condensation and that the thickness of the PFOMA layer can be adjusted to enable the fabrication of fully embedded Ag grids, thereby avoiding the need for a separate grid embedding step.

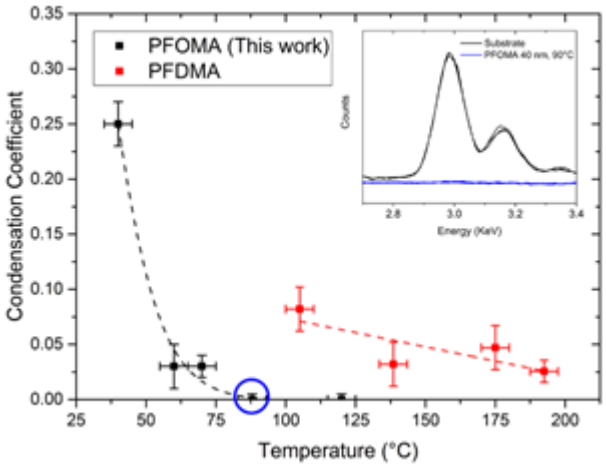

Figure 2: Graph showing C verses substrate temperature for a Ag thickness equivalent to 50 nm deposited at 2.7 Å s^{-1} onto printed areas of PFOMA (Black, this work) and PFDMA (Red).[43] Inset: Example EDXS analysis of the circled in Blue at 90°C where the Ag signal was below the detectable limit.

Whilst the factors affecting the process of spontaneous desorption of metal atoms (and thus *C*) from organic surfaces are still to be fully elucidated, it is evident from the small body of published work to date that whether or not an incident metal atom is adsorbed onto the organic surface or ejected back into the vacuum depends primarily on the strength of the attractive interaction between them.[42,43,53–57] Intuitively, the potential well depth associated with the attractive interaction must exceed the kinetic energy of the incident atom for the incident atom to remain bound to the surface. In the current context Ag is evaporated from a thermal source at temperature of ~ 958°C and so the average kinetic energy per atom, which is equal to the average thermal energy $(3/2)k_BT$, is ~ 0.16 eV. The very low surface energy of PFOMA films (11.1 ± 0.2 mJ m^{-2} (Table S1, Supporting Information)) is consistent with the perfluorinated chains on the polymethacrylate backbone being orientated towards the film surface[42] and these chains are expected to interact only very weakly with the incident Ag atoms due to: (i) the very high strength of the C-F bond, which makes it resistant to chemical reaction with the incident Ag atoms.; (ii) the electronegativity of F atoms, which results in the C-F bonds having exceptionally low polarizability and thus only very weak dispersive interactions with the incident Ag atoms. The energy of dispersive force interactions between gas atoms and solid surfaces is typically an order of magnitude lower than the kinetic energy of the incident Ag atoms in this case, which is consistent with the observation of low *C* for PFOMA.[58,59] Whilst the same is also true for the case of PFDMA, because it has a very similar structure and surface energy (10.1 ± 0.3 mJ m^{-2} (Supporting Information, Table S1)), it is clear from Figure 2 that PFOMA is far less susceptible to Ag adsorption than PFDMA: *C* is reduced to ~ 0.03 at 60°C as compared to ≥ 140°C for PFDMA, and reduces to zero when the substrate is heated to 90°C, which is not achieved for PFDMA. The fact that *C* on both polymers is temperature dependent but is far lower for the softer completely amorphous variant (as is determined from the force spectroscopy and differential scanning calorimetry shown in Figures S2 and S4) indicates that the difference in the ability to resist Ag condensation stems from a difference in the degree of movement of the

perfluorinated chains. Perfluorinated chains are known to interact only very weakly with one another as compared to their alkyl analogues due to the lower dispersive interactions between chains and so will likely be disordered and free to move.[60] The idea that molecular motion at the surface of organic films can suppress nucleation of condensing metal atoms and promote desorption has been discussed by T. Tsujioka *et al.*[54,55] for the deposition of magnesium on diarylethene surfaces and by our group[43] for the case of Ag on perfluorinated molecules. In the current context it is hypothesised that the movement of the perfluorinated chains hinders access of incident Ag atoms to the polymer back bone with which it would be expected to interact much more strongly, particularly at the site of the carbonyl groups.

Figure 3 (a) shows Ag grid electrodes with a range of pitches produced using a patterned 40 nm PFOMA layer with a substrate temperature of 120°C. The metal thickness is increased to 100 nm and the linewidth is 3 ± 1 μm (Supporting Information, Figures S7 and S8). For this Ag thickness the amount of Ag deposited on the PFOMA is below the resolution limit of EDXS and the grids are clear to the eye. However, upon inspection using scanning electron microscopy (SEM) tiny Ag nanoparticles are observed on the PFOMA covered area: Supporting Information Figure S9. It is well known that Ag nanoparticles as small as 2-3 nm in diameter can couple strongly with visible light due to the large absorption cross-section that results from excitation of localized surface plasmon resonances.[61] Consequently, there is a small attenuation of transmitted light peaking for wavelength of 450 nm: Supporting Information, Figure S10. However, as also shown in Figure S10, this parasitic optical loss is easily removed by brief UV/O_3 treatment followed by rinsing with acetic acid which oxides and dissolves the Ag nanoparticles respectively. Crucially, this treatment also oxidizes the PFOMA surface increasing its surface energy so that is can be wetted with the conducting polymer poly(3,4-ethylenedioxythiophene):poly(styrenesulfonate) PEDOT:PSS (PH1000), which is sufficiently conductive to span the gaps between grid lines even when very thin (< 30 nm). The substantial reduction in sheet resistance (e.g. from 8.3 to 6.0 Ω sq^{-1} for a 75 μm pitch grid) upon PEDOT:PSS deposition is attributed to an improvement in the crystallinity of the Ag grid lines upon heating at 120°C, since the PEDOT:PSS film alone has a sheet resistance > 1000 Ω sq^{-1}. Importantly there is no significant difference in performance between Ag grid | PEDOT:PSS electrodes fabricated on glass and flexible PET substrates and the performance of grids with a pitch of 75 μm exceeds that of ITO glass: FoM 470 *vs*. 400 (Supporting Information, Equation S1). To test the robustness of the grid towards repeated bending through a small radius of curvature a 5 × 5 cm area grid was fabricated on a flexible PET substrate and bent 100,000 times through a radius of curvature of 6 mm, after which the sheet resistance increased by 5% (Supporting Information, Figure S11). The Scotch tape adhesion test[62] was then applied three times to determine if delamination of the grid from the substrate had occurred as a result of repeated bending. Following this process the sheet resistance increased by less than 1%, which is compelling evidence that the grid lines remain strongly bound to the plastic substrate. In contrast the sheet resistance of commercial ITO coated flexible plastic increased by a factor of 30 times after only 100 bend cycles.

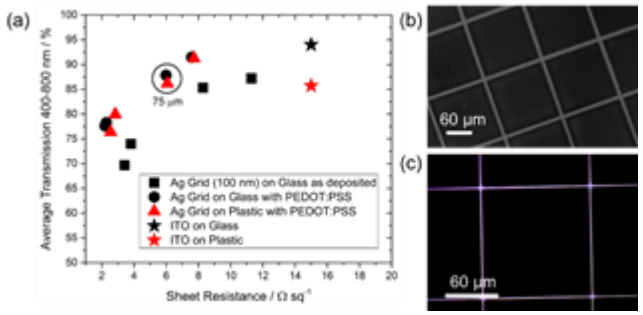

Figure 3:(a) Optoelectronic performance of a range of metal grid patterns with linewidth 3 ± 1 µm, metal thickness 100 nm and pitch as labelled (40, 50, 75 and 150 µm). The black points are translated as depicted by the arrow upon post-processing including a short exposure to O_3, application of PEDOT:PSS and subsequent annealing at 120°C. (b) SEM image of an example Ag grid, the white scale bar denotes 50 µm. Further examples are given in Supporting Information Figure S9. (c) Optical image of an example Ag grid, the white scale bar again denotes 50 µm.

To demonstrate the utility of optimized grid electrodes as a replacement for ITO glass in OPVs, Ag grid electrodes with a pitch of 75 µm, linewidth 3 ± 1 µm and a thin PEDOT:PSS interlayer of 25 nm were used in the device structure: Transparent Electrode | ZnO | PBDB-T/ITIC | MoO_3 | Al. The grid electrode with PFOMA in the gaps between gridlines was briefly UV/O_3 treated and rinsed with acetic acid before deposition of PEDOT:PSS to facilitate wetting of the electrode by the PEDOT:PSS layer. These electrodes have average transparency of 88% and sheet resistance of 6 Ω sq^{-1}. The model OPV devices in Figure 3 and Table 2 demonstrate the comparable performance of ITO and metal grids produced in this manner, with almost identical champion device performance (Figure 4) and the same average power conversion efficiencies within error of 9.9 ± 0.3% and 9.5 ± 0.7% respectively (Table S4, Supporting Information). Notably, even though the PFOMA thickness is substantially lower than the Ag line thickness (80 *vs* 100 nm), so the grid lines are not fully embedded, the device *FF* is not compromised; Table S4. The polymer thickness can however be tuned to match the thickness of the Ag grid lines.[43]

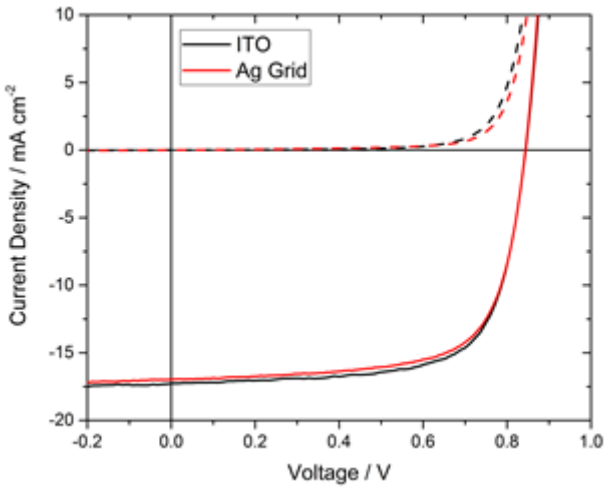

Figure 4: Champion ITO and Ag grid devices for the device structure Transparent Electrode | ZnO | PBDB-T/ITIC | MoO_3 | Al, tested under 1 sun simulated solar illumination (solid lines) and in the dark (dashed lines).

PEDOT:PSS is often considered to be a source of instability in OPVs due to it acidity and propensity to take up water,[63,64] and so we have explored the possibility of removing the PEDOT:PSS layer altogether. To avoid unacceptable resistive losses, this requires the distance between adjacent grid lines (i.e. the pitch) to be greatly reduced. To this end we have reduced the pitch to 10 µm and compensated as far as possible for the higher grid line density by reducing the linewidth by a factor of five to 600 ± 100 nm (Figure 5 (a) and Supporting Information Figure S12). For a Ag thickness of 100 nm this electrode has an average transparency of 85% and conductivity of 6.0 Ω sq^{-1} yielding a FoM of 401, which is equal to that of ITO glass. We have tested this electrode in an inverted device architecture using a commercial ZnO electron transport layer (Ossila Ltd), which has a conductivity 6 orders of magnitude below that of PEDOT:PSS (PH1000). The electrodes were rinsed with the perfluorinated solvent HFE-7500 (3M) to remove the PFOMA layer prior to ZnO deposition to ensure uniform wetting. The power conversion efficiency of model OPVs using this PEDOT:PSS free electrode is lower than that of identical devices using a conventional ITO glass electrode; 9.8 ± 0.5% *vs* 11.8 ± 0.7% due to a lower current and an increased series resistance; Figure 5 and Supporting Information Table S5. However this difference may prove acceptable if improvements in device stability resulting from the omission of the PEDOT:PSS are forthcoming.

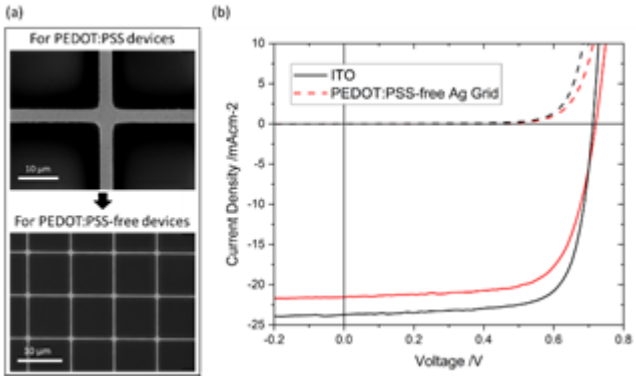

Figure 5: (a) SEM images (both scale bars 10 µm) highlighting the reduction in pitch and line width to enable PEDOT:PSS-free devices. (b) Champion ITO and PEDOT:PSS-free Ag grid devices for the device structure Grid/ITO | ZnO| PM6:Y6 | MoO_3 | Al. Please note that these devices are based on the PM6:Y6 bulk-heterojunction (a more modern derivative of PCE-12:ITIC) and so not directly comparable to the data in Figure 4.

In summary, a new perfluorinated polymer for the fabrication of high-performance transparent Ag grid electrodes by condensation coefficient modulation is reported. Optimized electrodes on glass and flexible plastic substrates have a figure-of-merit that exceeds that of commercial ITO glass, and when on plastic the grid electrode is remarkably stable towards repeated bending through a small radius of curvature. This young approach to the fabrication of Ag grid electrode is promising because it does not require chemical etchants, complex post-deposition transfer step or a separate grid embedding step. The performance of model solution processed OPV devices is shown to be unchanged when ITO glass is replaced with an optimised PEDOT:PSS coated Ag grid electrode, which we believe represents a substantive technological achievement.

Experimental

PFOMA synthesis

1*H*,1*H*,2*H*,2*H*-Perfluorooctyl methacrylate (FOMA, 99%) was procured from Shanghai Heat-Biochem Co., China, and used after passing through a short column packed with Al_2O_3. 2,2'-Azobisisobutyronitrile (AIBN, > 98.0%) was purchased from Junsei Chemical, Japan, and used after recrystallization from a mixed solvent of $CHCl_3$ and MeOH. Benzotrifluoride (BTF) was purchased from SigmaAldrich, USA.

Size exclusion chromatography (SEC) was performed on a Younglin GPC system (YL9100, equipped with a refractive index detector) by eluting AsahiKlin AK225G at 35°C.[65] Monodisperse poly(methyl methacrylate) (PMMA; molecular weight from 860 to 2,200,000; Showa-Denko, Japan) was used as a reference standard.

FOMA (10.0 g, 23.1 mmol), AIBN (0.20 g) and BTF (13 cm^3) were added into a Schlenk tube. It was sealed and degassed by three freeze-pump-thaw cycles under an N_2 atmosphere. The solution was

stirred magnetically for 15 h at 72°C under an N_2 atmosphere. The resulting viscous solution was added dropwise into stirring MeOH. The precipitate was filtered and dried under reduced pressure to yield 7.6 g of a white powder (76% yield).

Differential scanning calorimetry (DSC) was performed using a Mettler Toledo DSC 1 operating with the Star e software. The samples were run in a 40 µL aluminium standard pan with a pinhole placed in the lid to allow for gas escape. The samples were run at a heating rate of $10^{o}C\ min^{-1}$ and cooling was performed using liquid nitrogen.

Microcontact Printing

For the fabrication of grids with a 3 µm linewidth, a negative photoresist (AZ, nLOF 2035) was spun on to a 3" silicon wafer, baked and exposed to 90 mJ cm^{-2} UV light through a chromium mask patterned with the grid lines. The resultant wafer was baked post-exposure for 90s followed by development in MF-319 developer for 30s. 300 nm Al_2O_3 (99.99%, Kurt J. Lesker) was then evaporated across the wafer followed by lift off in acetone. The patterned wafer was etched in the Inductively Coupled Plasma (ICP) Etcher to a depth of 1.78 µm. The Al_2O_3 was removed using MF319 developer giving a raised silicon grid of 1.4 µm.

The resultant patterned silicon was silanized with (1H,1H,2H,2H-perfluorooctyl)trichlorosilane (FTS) under low pressure to aid release. Polydimethylsiloxane (PDMS, Sylgard 184) with a 10:1 w/w mixture of base and curing agent was then degassed and poured atop of the resultant master. After curing overnight at 80°C the PDMS replica 'stamp' was detached from the master: Both the stamps and master were used repeatedly throughout this work.

For the fabrication of grids with a sub-micron linewidth, the image reversal photoresist nLOF 5214 was used in its negative mode by being spun on to a 3" silicon wafer, baked, exposed to 60 mJ/cm^2, reversed baked for 2 minutes before being flood exposed to 250 mJ/cm^2 then developed in MF-319 for 30 s. The resulting grid pattern was etched in the ICP etcher to a depth of 600nm. The remaining resist was removed by Ashing in the ICP.

Grid fabrication

Glass or PET substrates were ultrasonically agitated in an aqueous surfactant (Hellmanex III) solution, deionized water only and then IPA for 15 minutes each with a subsequent 15-minute UV/O_3^- cleaning step immediately before use. PFOMA was dissolved at 2-8% w/w in HFE-7500 (3M) at room temperature, with 4% w/w resulting in a 40 nm polymer layer when printed and thicker solutions used to embed the metal lines and lower roughness. This solution was either spin coated to the stamp at 2000 rpm or covered and dried in a stream of nitrogen. With gentle pressure this was brought into contact with the substrate for < 2 seconds and then detached, leaving a reverse replica of the patterned silicon produced in PFOMA on the substrate. The stamp was reused immediately with no additional steps. 100 nm Ag was evaporated to these prepared substrates at 2.7 Å s^{-1} and at varied substrate temperature using a Mbraun thermal evaporator.

Characterisation and Measurement

SEM and EDX spectra were collected using a ZEISS Gemini500 with an integrated Si-Li detector unit (Oxford Instruments). An accelerating voltage of 2 kV for imaging and 10 kV for EDX analysis was used. For EDX analysis the electrodes were produced on silicon substrates to allow for accurate quantification of the metal content embedded in the polymer, and a ratio of Ag in the polymeric regions to the bare substrate used to present this (Condensation Coefficient, *C*). To calculate sheet resistance grid electrodes were fabricated and painted with silver contacts to connect a Keithley 2400 source meter. Resistances were calculated using the van der Pauw method at an applied voltage of 5 mV. The bend testing used a custom rig which flexes the freestanding electrode around a radius of 6 mm and the resistance was tested periodically. Transmission measurements were made using a Cary 60 UV-is spectrometer and referenced to the substrate to account for the reflection at the air-substrate interface. Topographical AFM imaging was performed by Asylum Research MFP-3D in tapping mode. Force curves for the drop-cast thick polymer films were obtained using the same instrument in contact mode with a silicon tip (spring constant: 2 nN/nm). The surface free energy components were calculated using the Owens, Wendt, Rabel and Kaelble (OWRK) method from static contact angle measurements on 2/0.9 µL droplets respectively of deionized water and n-hexadecane captured using a Krüss (DSA100) drop shape analysis system.[66,67]

Model OPV devices

For OPV devices using a PEDOT:PSS interlayer (Figure 4) PH1000 (Ossila) was diluted with 2 parts deionized water, filtered through a 0.45 µm filter and both dimethyl sulfoxide and Capstone FS-50 (a fluorinated surfactant to improve wetting, Chemours) added in 5% w/w quantities. The grid electrode as deposited is UV/O_3 treated for < 2 minutes and rinsed with glacial acetic acid before PEDOT:PSS is spin coated at 5000 rpm for 30 seconds and annealed at 120˚C. Under an inert atmosphere ZnO (aluminum-doped zinc oxide ink for spin coating/slot-die coating, Sigma Aldrich, filtered) was spin coated onto both the grid structure and ITO glass (Thin Film Devices) reference electrodes and annealed at 120˚C. A 20 mg/mL PBDB-T:ITIC solution was prepared in chlorobenzene with a 1:1 ratio of PBDB-T and ITIC before addition of 0.5% v/v 1,8-diiodooctane, spin coating and annealing at 120˚C. The device structures were then loaded to the thermal evaporator and 6 nm MoO_3 was evaporated at 0.2 Å s^{-1}. An aluminum cathode (100 nm) is then evaporated through a mask with an approximate device area of 0.07 cm^2. All devices were tested under inert atmosphere and 1 sun illumination through a calibrated shadow mask of aperture size 0.012 cm^2.

For the PEDOT:PSS-free OPV devices (Figure 5) grid electrodes were rinsed with HFE-7500 (3M) solvent to remove the PFOMA layer before ZnO was spin coated at 2000 rpm from a commercial nano-particle solution (aluminum-doped zinc oxide ink for spin coating/slot-die coating, Sigma Aldrich, filtered) and the electrodes annealed at 120˚C. An 18 mg/mL PM6:Y6 solution was prepared in chlorobenzene with a 1:1.2 ratio of PM6 and Y6. The additives chloronaphthalene (1.25% v/v) and diphenyl ether (0.5% v/v) were added immediately prior to spin coating at 3000 rpm and annealing at 80˚C. The device structures were then loaded into the thermal evaporator and 6 nm MoO_3 was evaporated at 0.2 Å s^{-1}. An aluminum cathode (100 nm) is then evaporated through a mask with an approximate device area of 0.07 cm^2. All devices were tested under inert atmosphere and 1 sun illumination through a calibrated shadow mask of aperture size 0.012 cm^2.

Supporting Information

All data supporting this study are provided as the supporting information accompanying this paper.

Acknowledgments

The authors would like to thank Dr James Town of the University of Warwick for collecting the differential scanning calorimetry data shown in Supporting Information Figure S4.

Funding

The authors would like to thank the United Kingdom Engineering and Physical Sciences Research Council (EPSRC) for funding (grant number: EP/V002023/1).

References

[1] A. Singh, A. Singh, *Solar Energy Capture Materials* (Ed.: Gibson, E. A.), Royal Society of Chemistry, Cambridge, **2019**.

[2] K. L. Wang, Y. H. Zhou, Y. H. Lou, Z. K. Wang, *Chem Sci* **2021**, *12*, 11936.

[3] E. Pascual-San José, A. Sánchez-Díaz, M. Stella, E. Martínez-Ferrero, M. I. Alonso, M. Campoy-Quiles, *Sci Technol Adv Mater* **2018**, *19*, 823.

[4] H. S. Ryu, S. Y. Park, T. H. Lee, J. Y. Kim, H. Y. Woo, *Nanoscale* **2020**, *12*, 5792.

[5] V. Pecunia, L. G. Occhipinti, R. L. Z. Hoye, *Adv Energy Mater* **2021**, *11*.

[6] M. Ylikunnari, M. Välimäki, K. L. Väisänen, T. M. Kraft, R. Sliz, G. Corso, R. Po, R. Barbieri, C. Carbonera, G. Gorni, M. Vilkman, *Flexible and Printed Electronics* **2020**, *5*.

[7] B. Lee, L. Lahann, Y. Li, S. R. Forrest, *Sustain Energy Fuels* **2020**, *4*, 5765.

[8] D. Hengevoss, C. Baumgartner, G. Nisato, C. Hugi, *Solar Energy* **2016**, *137*, 317.

[9] Y. Li, X. Huang, K. Ding, H. K. M. Sheriff, L. Ye, H. Liu, C. Z. Li, H. Ade, S. R. Forrest, *Nat Commun* **2021**, *12*, 1.

[10] F. Yang, Y. Huang, Y. Li, Y. Li, *npj Flexible Electronics 2021 5:1* **2021**, *5*, 1.

[11] X. Wang, Q. Sun, J. Gao, J. Wang, C. Xu, X. Ma, F. Zhang, *Energies (Basel)* **2021**, *14*.

[12] H. Lu, X. Ren, D. Ouyang, W. C. H. Choy, W. C. H Choy, H. Lu, X. Ren, D. Ouyang, W. C. H Choy, *Small* **2018**, *14*, 1703140.

[13] N. G. Park, *Adv Energy Mater* **2020**, *10*, 1903106.

[14] V. Zardetto, T. M. Brown, A. Reale, A. di Carlo, *J Polym Sci B Polym Phys* **2011**, *49*, 638.

[15] Y. Wang, C. Zhu, R. Pfattner, H. Yan, L. Jin, S. Chen, F. Molina-Lopez, F. Lissel, J. Liu, N. I. Rabiah, Z. Chen, J. W. Chung, C. Linder, M. F. Toney, B. Murmann, Z. Bao, *Sci Adv* **2017**, *3*.

[16] P. Bellchambers, S. Varagnolo, C. Maltby, R. A. Hatton, *ACS Appl Energy Mater* **2021**, *4*, 4150.

[17] D. A. Jacobs, K. R. Catchpole, F. J. Beck, T. P. White, *J Mater Chem A Mater* **2016**, *4*, 4490.

[18] L. Yin, Z. Zhao, F. Jiang, Z. Li, S. Xiong, Y. Zhou, *Org Electron* **2014**, *15*, 2593.

[19] X. Fan, W. Nie, H. Tsai, N. Wang, H. Huang, Y. Cheng, R. Wen, L. Ma, F. Yan, Y. Xia, *Advanced Science* **2019**, *6*.

[20] D. Ebner, M. Bauch, T. Dimopoulos, *Opt Express* **2017**, *25*, A240.

[21] J. Yun, *Adv Funct Mater* **2017**, *27*, 1606641.

[22] H. Kang, S. Jung, S. Jeong, G. Kim, K. Lee, *Nat Commun* **2015**, *6*, 6503.

[23] O. S. Hutter, R. A. Hatton, *Advanced Materials* **2015**, *27*, 326.

[24] H. Zhang, R. Liu, S. Guo, Z. Wang, X. Sun, J. Lin, Q. Luo, C. Ma, *Org Electron* **2022**, *100*, 106352.

[25] H. G. Im, S. H. Jung, J. Jin, D. Lee, J. Lee, D. Lee, J. Y. Lee, I. D. Kim, B. S. Bae, *ACS Nano* **2014**, *8*, 10973.

[26] W. Cao, J. Li, H. Chen, J. Xue, *J Photonics Energy* **2014**, *4*, 040990.

[27] K. Zilberberg, T. Riedl, *J. Mater. Chem. A* **2016**, *4*, 14481.

[28] C. P. Muzzillo, *Solar Energy Materials and Solar Cells* **2017**, *169*, 68.

[29] M. Morales-Masis, S. de Wolf, R. Woods-Robinson, J. W. Ager, C. Ballif, *Adv Electron Mater* **2017**, *3*.

[30] Y. Sun, M. Chang, L. Meng, X. Wan, H. Gao, Y. Zhang, K. Zhao, Z. Sun, C. Li, S. Liu, H. Wang, J. Liang, Y. Chen, *Nature Electron* **2019**, *2*, 513.

[31] C. Mayousse, C. Celle, A. Fraczkiewicz, J.-P. Simonato, *Nanoscale* **2015**, *7*, 2107.

[32] H. H. Khaligh, I. A. Goldthorpe, *Nanoscale Res Lett* **2013**, *8*, 235.

[33] T. Wang, C. Luo, F. Liu, L. Li, X. Zhang, Y. Li, E. Han, Y. Fu, Y. Jiao, *Langmuir* **2017**, 33, 4702.

[34] Y. Li, L. Meng, Y. Yang, G. Xu, Z. Hong, Q. Chen, J. You, G. Li, Y. Yang, Y. Li, *Nat Commun* **2016**, *7*, 10214.

[35] Y. Li, L. Mao, Y. Gao, P. Zhang, C. Li, C. Ma, Y. Tu, Z. Cui, L. Chen, *Sol Energy Mater Sol Cells* **2013**, *113*, 85.

[36] N. C. Raut and K. Al-Shamery, *J. Mater. Chem. C* **2018**, *6*, 1618.

[37] T.-S. Choi, D. W. Hess , *ECS J. Solid State Sci. Technol.*, **2015**, *4* , 3084.

[38] F.-T. Zhang , L. Xu , J.-H. Chen , B. Zhao , X.-Z. Fu , R. Sun , Q. Chen and C.-P. Wong, *ACS Appl. Mater. Interfaces* **2018**, 10 , 2075.

[39] L. Zhao, D. Chen, W. Hu, *Langmuir* **2016** *32* , 5290.

[40] H. B. Lee, W-Y. Jin, M. M. Ovhal, N.Kumar, J-W. Kang, *J. Mater. Chem. C 2019*, 7, 1087.

[41] Y. Yang, F. Min, Y. Qiao, Z. Li, F. Vogelbacher, Z. Liu, W. Lv, Y. Wang, Y. Song, *Nano Energy* **2021**, *89*, 106384.

[42] S. Varagnolo, J. Lee, H. Amari, R. A. Hatton, *Mater Horiz* **2020**, *7*, 143.

[43] S. Varagnolo, K. W. Park, J. K. Lee, R. A. Hatton, *J Mater Chem C Mater* **2020**, *8*, 13453.

[44] J. A. Helmuth, H. Schmid, R. Stutz, A. Stemmer, H. Wolf, *J Am Chem Soc* **2006**, *128*, 9296.

[45] C. Merian, D. E. Hardt, X. Du, H. AlQahtani, In *ASME 2015 International Mechanical Engineering Congress and Exposition*, MIT, Houston, Texas, **2015**, pp. 1–7.

[46] T. W. Odom, J. C. Love, D. B. Wolfe, K. E. Paul, G. M. Whitesides, *Langmuir* **2002**, *18*, 5314.

[47] Y. Xia, G. M. Whitesides, *Langmuir* **1997**, *13*, 2059.

[48] H. A. Biebuyck, N. B. Larsen, E. Delamarche, B. Michel, *IBM J Res Dev* **1997**, *41*, 159.

[49] M. S. Kim, D. H. Lee, Y. H. Cha, K. B. Kim, S. H. Jung, J. K. Lee, O. Beom-Hoan, S. G. Lee, S. G. Park, *Microelectron Eng* **2014**, *123*, 33.

[50] K. Hashizaki, Y. Hoshii, K. Ikeuchi, M. Imai, H. Taguchi, Y. Goto, M. Fujii, *Chem. Pharm. Bull* **1083**, *69*, 1083.

[51] T. Çaykara, M. G. Sande, N. Azoia, L. R. Rodrigues, C. J. Silva, *Med Microbiol Immunol* **2020**, *209*, 363.

[52] L.-J. Pegg **2012,** Controlling hole extraction in organic photovoltaics. PhD Thesis. University of Warwick.

[53] T. Tsujioka, *Chemical Record* **2016**, *16*, 231.

[54] T. Tsujioka, Y. Sesumi, R. Takagi, K. Masui, S. Yokojima, K. Uchida, S. Nakamura, *J Am Chem Soc* **2008**, *130*, 10740.

[55] T. Tsujioka, R. Shirakawa, S. Matsumoto, R. Nishimura, K. Uchida, *Journal of Vacuum Science & Technology A: Vacuum, Surfaces, and Films* **2017**, *35*, 020603.

[56] T. Tsujioka, K. Tsuji, *Applied Physics Express* **2012**, *5*, 021601.

[57] T. Tsujioka, H. Kusaka, *Adv Mater Interfaces* **2022**, *9*, 2201096.

[58] C. Wagner, N. Fournier, V. G. Ruiz, C. Li, K. Müllen, M. Rohlfing, A. Tkatchenko, R. Temirov, F. S. Tautz, *Nat Commun* **2014**, *5*.

[59] S. Kawai, A. S. Foster, T. Björkman, S. Nowakowska, J. Björk, F. F. Canova, L. H. Gade, T. A. Jung, E. Meyer, *Nat Commun* **2016**, *7*.

[60] X. Liu, J. G. Riess, M. P. Krafft, *Bulletin of the Chemical Society of Japan* **2018**, *91*, 846.

[61] D. U. Karatay, M. Salvador, K. Yao, A. K. Y. Jen, D. S. Ginger, *Appl Phys Lett* **2014**, *105*, 033304.

[62] M. Rezaee, L. C. Tsai, M. I. Haider, A. Yazdi, E. Sanatizadeh & N. P. Salowitz. *Sci Rep* **2019**, *9*, 19805.

[63] B. Ecker, J. C. Nolasco, J. Pallarés, L. F. Marsal, J. Posdorfer, J. Parisi, E. von Hauff, *Adv Funct Mater* **2011**, *21*, 2705.

[64] J. Cameron, P. J. Skabara, *Mater. Horiz.*, **2020**, *7*, 1759.

[65] T. Isemura, R. Kakita, K. Kawahara, *J Chromatogr A* **2004**, *1026*, 109.

[66] S. A. Paniagua, P. J. Hotchkiss, S. C. Jones, S. R. Marder, A. Mudalige, F. S. Marrikar, J. E. Pemberton, N. R. Armstrong, *Journal of Physical Chemistry C* **2008**, *112*, 7809.

[67] K. X. Ma, C. H. Ho, F. Zhu, T. S. Chung, *Thin Solid Films* **2000**, *371*, 140.

High performance silver grid electrodes on glass and plastic substrates fabricated by condensation coefficient modulation, using a perfluorinated polymer shown to be far superior to other compounds used for this purpose to date. The very narrow line-width and small pitch opens the door to using these electrodes in organic photovoltaics without a PEDOT:PSS layer to span the gaps between grid-lines.

Table of Contents Graphic